## POLITECNICO DI TORINO
## Repository ISTITUZIONALE

Covalent functionalization enables good dispersion and anisotropic orientation of multi-walled carbon nanotubes in a poly(l-lactic acid) electrospun nanofibrous matrix boosting

(Article begins on next page)

29 March 2023

# Accepted Manuscript

Covalent functionalization enables good dispersion and anisotropic orientation of multi-walled carbon nanotubes in a poly(L-lactic acid) electrospun nanofibrous matrix boosting neuronal differentiation

Nicola Vicentini, Teresa Gatti, Patrizio Salice, Giorgia Scapin, Carla Marega, Francesco Filippini, Enzo Menna

Please cite this article as: N. Vicentini, T. Gatti, P. Salice, G. Scapin, C. Marega, F. Filippini, E. Menna, Covalent functionalization enables good dispersion and anisotropic orientation of multi-walled carbon nanotubes in a poly(L-lactic acid) electrospun nanofibrous matrix boosting neuronal differentiation, Carbon (2015), doi: 10.1016/j.carbon.2015.08.094.

# Covalent functionalization enables good dispersion and anisotropic orientation of multi-walled carbon nanotubes in a poly(L-lactic acid) electrospun nanofibrous matrix boosting neuronal differentiation

Nicola Vicentini,[a] Teresa Gatti,[a] Patrizio Salice,[a] Giorgia Scapin,[b] Carla Marega,[a] Francesco Filippini,[b] Enzo Menna[a,*]

[a] Dipartimento di Scienze Chimiche, Università di Padova, via F. Marzolo 1, 35131, Padova, Italy

[b] Dipartimento di Biologia, Università di Padova, via U. Bassi 58/B, 35131, Padova, Italy

[*] Corresponding author.

E-mail address: enzo.menna@unipd.it

ABSTRACT

A biocompatible porous scaffold obtained *via* electrospinning a nanocomposite solution of poly(L-lactic acid) and 4-methoxyphenyl functionalized multi-walled carbon nanotubes is presented here for the first time for the enhancement of neurites outgrowth. Optimization of blend preparation and deposition parameters paves the way to the obtainment of defect-free random networks of nanofibers with homogeneous diameters ranging within the hundreds nanometers length scale. The tailored covalent functionalization of nanotubes surfaces allows a homogeneous dispersion of the nanofillers within the polymer matrix, diminishing their natural tendency to aggregate and form bundles. This results in a remarkable effect on the crystallization temperature, as evidenced through differential scanning calorimetry. Furthermore, transmission electron microscopy shows carbon nanotubes anisotropically aligned along the fiber axes, a feature believed to enhance neurites adhesion and growth. Indeed, microscopy images show neurites extension along the direction of nanofibers, highlighting the extreme relevance of scaffold morphology in engineering complex tissue environments. Furthermore, a remarkable effect on increasing the neurite outgrowth results when using the fibrous scaffold containing dispersed carbon nanotubes in comparison with an analogous one made of only polymer, providing further evidence of the key role played by carbon nanostructures in inducing neuronal                                           differentiation.

# 1. Introduction

Among biocompatible, FDA approved, polymeric materials, poly(L-lactic-acid) (PLLA) has attracted great attention since many years for a large number of practical applications, ranging from consumer products, to packaging and biomedicine [1]. Due to its renewable origin, excellent mechanical properties and transparency, it is widely recognized as a green alternative to other commonly used thermoplastics such as polystyrene and PET. Furthermore, the possibility to employ it as the matrix, in conjunction with different types of nanofillers, in polymeric nanocomposites (PNCs), paves the way to the obtainment of high-value functional materials, useful for a plethora of different scopes [2]. In principle, functional materials based on PNCs are expected not only to combine native features of basic components but also to eventually generate new promising ones. In this context, the use of carbon nanostructures (CNSs), including buckyballs, single and multi-walled carbon nanotubes (SWCNTs, MWCNTs), carbon nanohorns, or graphene-based materials, as nanofillers is very promising, being these nanomaterials largely attractive for several peculiarities, such as the high aspect ratio and the optimal electrical and thermal conductivities coupled to mechanical strength [3,4]. For this reason, they were

employed as active materials in many bioengineering applications [5,6].

Particularly, from the combination of PLLA with MWCNTs, we recently reported on the obtainment of a free-standing functional biocompatible scaffold, which has been used to induce neuronal differentiation from precursor cells [7]. Indeed, such a scaffold allowed us to make use of the widely recognized neuritogenetic properties of CNTs [8,9] while, at the same time, overcoming concerns related to CNS toxicity [10,11] being the concentration of potentially toxic nanomaterials very low. This way, the risk for *in vivo* cell damage due to CNS uptake is extremely reduced when considering that entrapment of CNSs within a slowly biodegradable polymer matrix does not allow for a massive release and uptake of nanofillers.

A key step for the preparation of the PNC scaffold was the organic covalent functionalization of pristine MWCNTs with 4-methoxyphenyl substituents (MWCNT-PhOMe) carried out through an *in situ* diazotization reaction in the presence of 4-methoxyaniline and isopentylnitrite [12]. Indeed, the decoration of the pristine nanotubes with organic moieties allowed overcoming the main problem related to their use as nanofillers in polymer matrices, which is the pronounced tendency to form aggregates and bundles, because of the strong van der Waals mutual interactions between

their sp$^2$-carbon networks. In addition, from a toxicological perspective, functionalization prevents the formation of intracellular aggregates [13], i.e. potentially dangerous structures, in case some cell eventually incorporate CNSs released from polymer matrix. Although covalent attachment of substituents might modify CNS morphologies by making surfaces less accessible, we demonstrated that it is possible to exert a good control on the morphological outcome of diazotization reactions by tuning the proportion of reagents and reaction times [12,14]. Furthermore, such a covalent functionalization, by affording CNS derivatives dispersible in organic solvents without the need for surfactants or additives, makes low-cost solution processing an effective alternative to other techniques for the production of PNCs, such as high temperature melt-blending.

Here we present a novel MWCNT-PhOMe@PLLA PNC scaffold (eCNT-PLLA), consisting of a 3D network of functional nanofibers, obtained through the electrospinning technique. In this case, covalent functionalization not only provides MWCNTs the ability to form stable PNC solutions in combination with PLLA, that is required for an effective electrospinning process, but also promotes their disentanglement and homogeneous dispersion in the resulting fibers. This approach is not new; in fact the use of oxidized SWCNTs

esterified with long alkyl chains was previously reported by Haddon and coworkers to produce PNCs fibers of polystyrene [15]. Covalent functionalization of the carbon nanomaterial enabled the effective electrospinning of the PNC solution, though the resulting fibrous material contained bundles of CNTs within the polymer matrix, meaning that a non-ideal dispersion was achieved. More biomedical applications of electrospun CNS-polymer composites have been reported also very recently [16].

The highly porous morphology obtained through electrospinning is expected to better mimic the environment in which neurons normally develop [17]. In particular, the obtained geometry is similar in scale and 3D arrangement to the collagen and laminin fibrils of the extracellular matrix (ECM) [18]. This aspect has fundamental implications in the further refinement of our bioengineering capability to mimic the neural environment. Moreover, the presence of MWCNTs within the PLLA matrix is thought to (i) locally reduce the polymer electrical resistance at the nanoscale level which enhances neuronal network activity [19,20] and (ii) to feature nanoscale meshwork within the polymer, hence providing fibers with an optimal surface nanoroughness and texture, ideal for cell adhesion and protein/growth factor retention [21,22].

## 2. Experimental

All reagents and solvents were purchased from Sigma-Aldrich and used as received if not otherwise specified. MWCNTs produced by Arkema were purchased by Sigma-Aldrich and were purified according to an already reported procedure [12]. Functionalization of MWCNT-PhOMe was carried out following the previously reported diazotization procedure [12], with slight modifications. For the sake of clarity, details are given below.

A dispersion of purified MWCNTs (10.2 mg, 0.849 mmol of C) in 1-cyclohexyl-2-pyrrolidone (CHP) (7 mL), pre-sonicated for 10 minutes (power level: 2.0, pulse on: 3 sec, pulse off: 3 sec) was transferred to a two-necked round-bottomed flask. A solution of 4-methoxyaniline (58.1 mg, 0.472 mmol) in 3 mL of CHP was added and the mixture was heated to 80 °C under a nitrogen atmosphere. Then, isopentylnitrite (47.9 mg, 0.409 mmol) was added carefully. After 15 minutes of continuous stirring, the reaction mixture was diluted with methanol (100 mL) and centrifuged (2 x 5 minutes at 3000 rpm). The supernatant was removed and the precipitate was washed with methanol (1 x 7 mL) and recovered again through centrifugation and supernatant removal.

The black carbonaceous solid was dried under an IR lamp for 30 minutes. Then, it was split into two portions and each one was subjected to an extraction procedure, respectively in chloroform and DMF. Specifically, extraction

profiles in the two solvents (see S.I.) were obtained by sonication (power level: 2.0, pulse on: 3 sec, pulse off: 3 sec, 5 min) in 7 mL of solvent, followed by centrifugation (3000 rpm, 5 min) and removal of the supernatant, which was subjected to UV-Vis-NIR analysis. The sequence was repeated on the remaining solid precipitate at the bottom of the centrifugation vessel for five times. The first fractions were subjected to TGA and micro-Raman analysis (see S.I.) [12]. Dynamic light scattering (DLS) measurements were also performed on this fractions dispersed in air equilibrated solvents with a Zetasizer Nano S (Malvern Instruments) at 20 °C, by setting 20 runs of 10 seconds for each measurement, in order to determine mean solvodynamic diameters of the aggregates present in solution (see S.I.). Stability of solutions to re-aggregation was evaluated by monitoring the NIR absorbance at 1000 nm over a period of 12 h (see S.I.).

MWCNT-PhOMe@PLLA solutions in 9:1 $CHCl_3$:DMF (v/v) were prepared by adding a dispersion of MWCNT-PhOMe in DMF obtained through sonication (power level: 2.0, pulse on: 3 sec, pulse off: 3 sec, 5 min) to a chloroform solution of PLLA under continuous stirring, followed by a centrifugation step aimed at removing residual aggregates (4500 rpm, 15 min) (see S.I.). The small DMF portion in the solvent was introduced to increase the boiling point, i.e. to optimize conditions for electrospinning.

Electrospinning was performed on a home-made apparatus with an applied voltage of 18 kV, tip to collector distance of 20 cm and by maintaining a solution flow rate of 0.03 mL min$^{-1}$ on the syringe pump injector. Scanning electron microscopy (SEM) images of electrospun nanofibers were obtained on a Jeol JSM 6490 instrument. Transmission electron microscopy (TEM) images were recorded on a Tecnai G$^2$ (FEI) microscope operating at 100 kV. Images were captured with a Veleta digital camera (Olympus soft imaging system). Differential scanning calorimetry (DSC) measurements were carried out with a DSC Q20 (TA Instruments) under nitrogen by heating the samples at 1 °C min$^{-1}$ over a temperature range from 50 to 180 °C.

The biological properties of the fibrous scaffold were analyzed by evaluating the viability/proliferation and differentiation of SH-SY5Y cells, a neuroblastoma cell line that resemble immature neuroblasts in being locked at an early neuronal differentiation stage but that can be easily differentiated toward the neuronal phenotype by retinoic acid (RA) treatment [23].

For space constraints, a shortened version of biological methods is presented hereafter, while full methods are included in the S.I. file. SH-SY5Y cells were cultured as reported [7]. Scaffolds were incubated (24 hours) in the growth medium prior to seeding cells onto either the scaffolds or control well bottoms.

Twenty-four hours after cell seeding (day 0), the culture medium was replaced by the differentiation medium (see S.I.) supplemented with 10 μM all-*trans*-retinoic acid (RA). In undifferentiated control samples, Dimethyl sulfoxide was added as equivalent amount (in which RA is dissolved). Analysis of cell viability/proliferation and of ability to adhere to the scaffolds were performed as reported, using the Resazurin reduction assay to quantify metabolically active cells [7]. Background values from blank samples were subtracted and average values for the duplicates calculated. Cell proliferation was calculated from a calibration curve by linear regression. Cell death was quantified via lactate dehydrogenase (LDH) assay and calculated from a calibration curve by linear regression after 100% cell lysis of known cell quantities. Cytotoxicity (%) was calculated as (number of dead cells)/(n of dead cells + number of living cells) x100. Neurite outgrowth was measured as reported [7] by staining cells with cell permeable calcein acetoxymethyl ester (Calcein-AM), which in living cells is converted by intracellular esterases to the strongly green fluorescent calcein. Each experiment was performed in duplicate (two wells per condition). Five images/well were recorded (ten images per condition). Neurite length was measured using LAS AF lite software (Leica) by tracing the trajectory of the neurite from the tip to the junction between the neurite and

cell body. If a neurite exhibited branching, the measurement from the end of the longest branch to the soma was recorded, then each branch was measured from the tip of the neurite to the neurite branch point. Neuritogenic properties were analyzed in terms of total neurite length/no. of cells (considering only neurites longer than 50 μm). See S.I. for details on statistical analysis. Values are expressed as mean ± standard error of the mean (M ± SEM).

## 3. Results and discussion

In order to proceed with the preparation of MWCNT-PhOMe@PLLA solutions suitable for electrospinning, reaction conditions for the *in situ* diazotization of pristine MWCNTs with 4-methoxyaniline have been optimized with the aim of maximizing dispersion of MWCNT-PhOMe in chloroform, a good solvent for PLLA. A solubility of up to 0.7 mg mL$^{-1}$ has been obtained. Stability of the solutions to re-aggregation was evaluated by monitoring the NIR absorbance at 1000 nm over a period of 12 h (see S.I.). Absorbance, i.e. concentration, decreased by less than

0.1%. A functionalization degree (FD) [24] of 1/33 has been evaluated *via* thermogravimetric analysis (TGA) (see S.I.).

A systematic screening was conducted by varying PLLA concentrations from 4 to 12% (w/w). Weight percentage of MWCNT-PhOMe with respect to PLLA was maintained constant for all polymer concentrations to 0.25% (w/w), ensuring a low content of CNSs in the resulting PNC material, in order to minimize toxicity issues. All PNC solutions thus prepared were spun onto glass slides by taking care of optimizing conditions in terms of applied voltage, flow rate and distance between the needle and the collecting plate. From the two most concentrated PLLA solutions (10% and 12% respectively) fibers with diameters of a few microns were obtained (see S.I.), but the process was generally less efficient compared to the use of more diluted solutions (6% and 8% respectively). From the lowest concentration solution (4%) no fibers were obtained, likely due to insufficient viscosity of the solution. We found an optimized trade-off between fibers quantities, diameters and defects with the 6% solution.
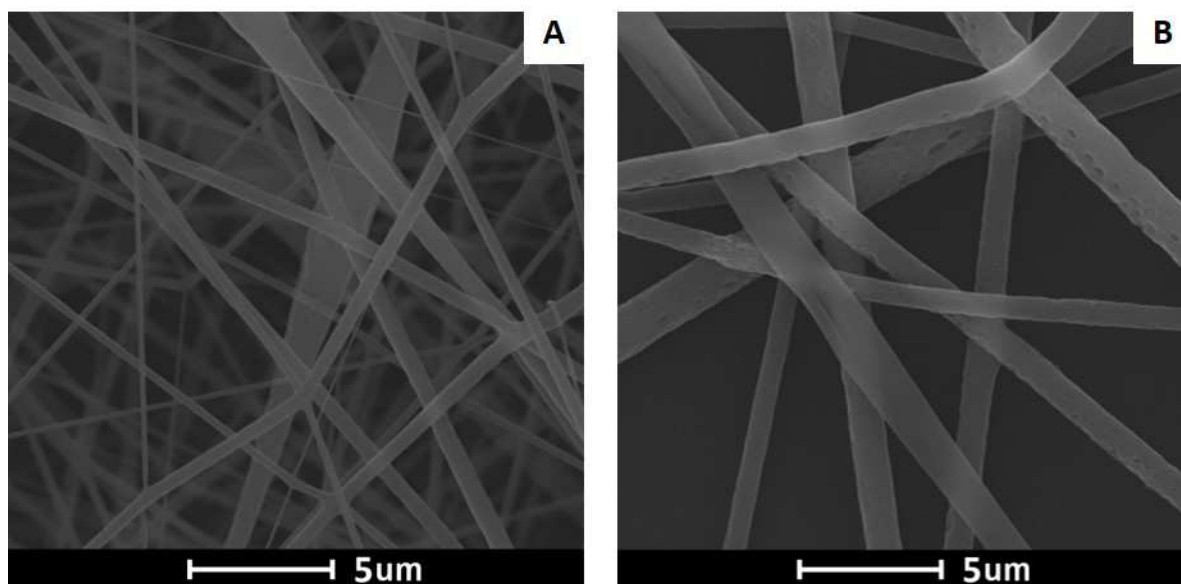
**Fig. 1 - SEM images of electrospun nanofibers obtained from (A) 6% MWCNT-PhOMe@PLLA solution and (B) 8% MWCNT-PhOMe@PLLA solution.**
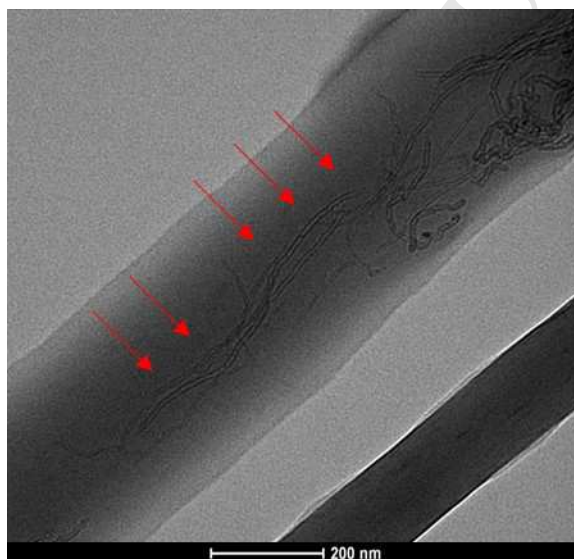


**Fig. 2 – TEM image of electrospun nanofibers obtained from 6% MWCNT-PhOMe@PLLA solution. Red arrows indicate regions of CNTs aligned along the fiber's axis.**

In these conditions, diameters of the resulting fibers were comprised between 200 and 600 nm, as evident from SEM images (Fig. 1A). The 8% solution also furnished good quality fibers, but in much smaller quantity, thus resulting in a lower density scaffold (Fig. 1B). TEM images of nanofibers from 6% MWCNT-PhOMe@PLLA solution collected on copper grids show the presence of regions containing unbundled nanotubes mainly aligned along the fiber axis direction (Fig. 2). We expect such anisotropy induced in the functional scaffold at the nanoscale level, likely as a result of the applied electrospinning voltage, to contribute significantly to the enhancement of its neuritogenetic response, by possibly providing specific sites with a suitable

nanotexture for neuron growth on the fibrous       matrix and local

**Table 1 – Calorimetric data for the functional scaffolds obtained via DSC analysis.**

|        | Scaffold | $T_c$ [°C] | $\Delta H_c$ [J g$^{-1}$][a] | $T_m$ [°C] | $\Delta H_m$ [J g$^{-1}$][a] | CD [%][b] |
|--------|----------|-----------|--------------|-----------|--------------|-----------|
| **Films** | PLLA | / | / | 155,4 | 28,2 | 30 |
|        | CNT-PLLA | / | / | 155,6 | 27,8 | 30 |
| **Fibers** | ePLLA | 85,7 | 16,0 | 152,2 | 27,5 | 12 |
|        | eCNT-PLLA | 80,9 | 17,4 | 151,4 | 28,4 | 12 |

a) Calculated from peak area. b) Degree of crystallinity calculated by comparison with theoretical data for 100% crystalline PLLA [21].
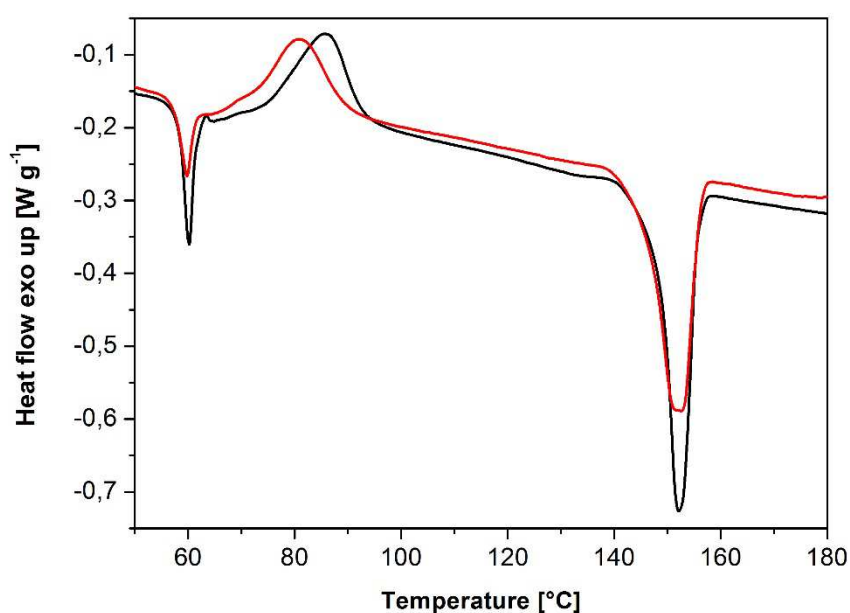


**Fig. 3 – DSC heating traces of ePLLA (black line) and eCNT-PLLA (red line) obtained at 1 °C min$^{-1}$ rate.**

continuous CNT pathways that could improve conductivity along each fiber (bulk resistivity have been found to decrease by 6 times in the presence of 0.25% CNTs; see Tab. S1).

DSC analysis allowed us to determine the degree of crystallinity (CD) of the eCNT-PLLA scaffold obtained from 6% MWCNT-PhOMe@PLLA solution. In this case CD was found to be 12%, by comparison with a theoretical value of crystallization enthalpy calculated for a 100% crystalline PLLA

sample (see Table 1) [25]. This value resulted lower with respect to the corresponding bulk PNC scaffold (CNT-PLLA) obtained *via* slow solvent evaporation on a heated plate (50 °C) (CD = 30%, see Table 1 and S.I.). Indeed, the fast solidification process occurring during electrospinning does not result in proper crystallization of the PNC material [26,27]. Thermograms higlight an important effect over fibers crystallization temperature ($T_c$) due to the presence of well-dispersed

MWCNT-PhOMe within the polymer matrix (Fig. 3). MWCNT-PhOMe acts as nucleating agent and thus tend to lower the $T_c$ [25]; in the case we report here, a 5 °C shift between neat PLLA nanofibers scaffold (ePLLA) and eCNT-PLLA
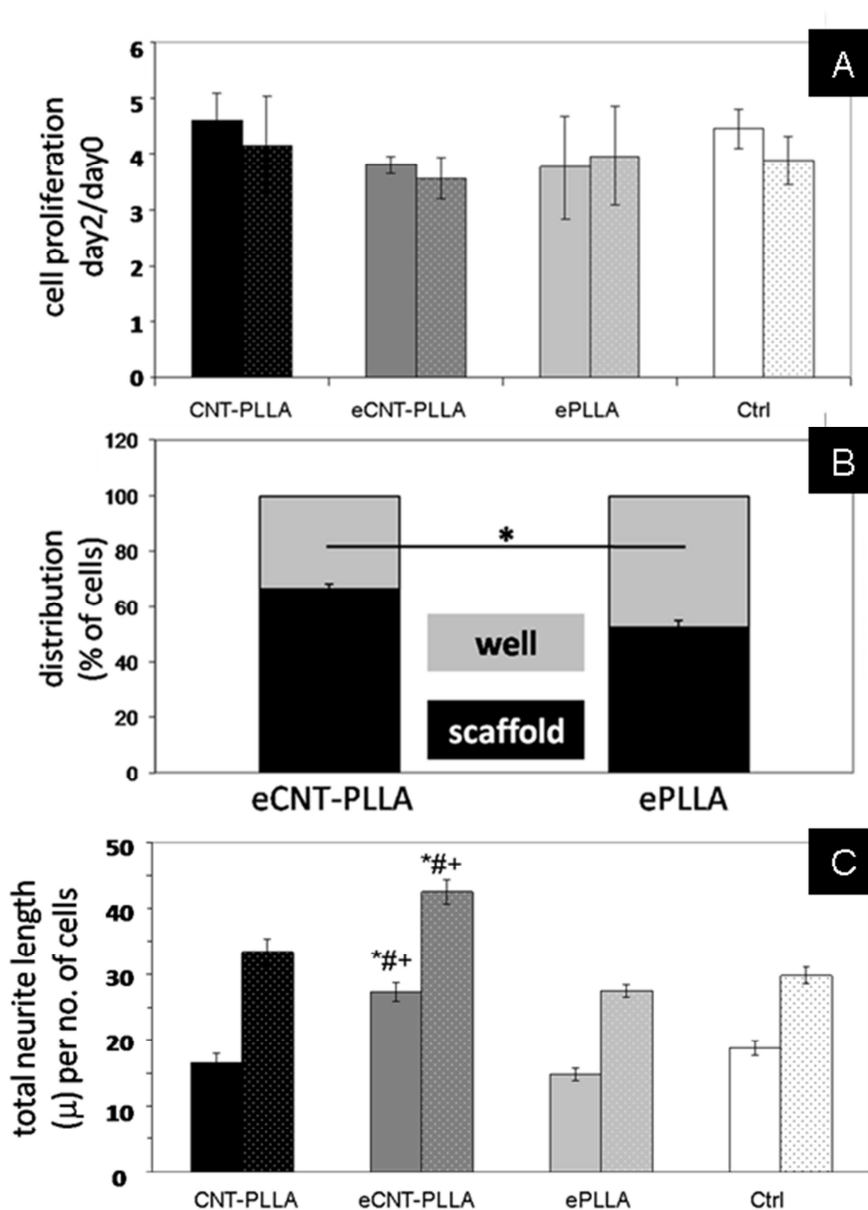


Fig. 4 - eCNT-PLLA scaffold effect on SH-SY5Y cell adhesion, growth and differentiation. (A) cell proliferation; (B) cell distribution and (C) cell differentiation. Data represent the mean ± SEM of three independent experiments performed in duplicate. (*) shows significance at p<0.05 between cells seeded onto eCNT-PLLA scaffolds and control (poly-L-lysine coated wells). (#) shows significance at p<0.05 between cells seeded onto eCNT-PLLA scaffolds and ePLLA scaffolds. (+) shows significance at p<0.05 between cells seeded onto CNT-PLLA scaffolds and eCNT-PLLA/ePLLA scaffolds. Dotted bars refer to the corresponding RA treated samples.

**Table 2 – Percentage of cell death relative to three independent experiments performed in duplicate**

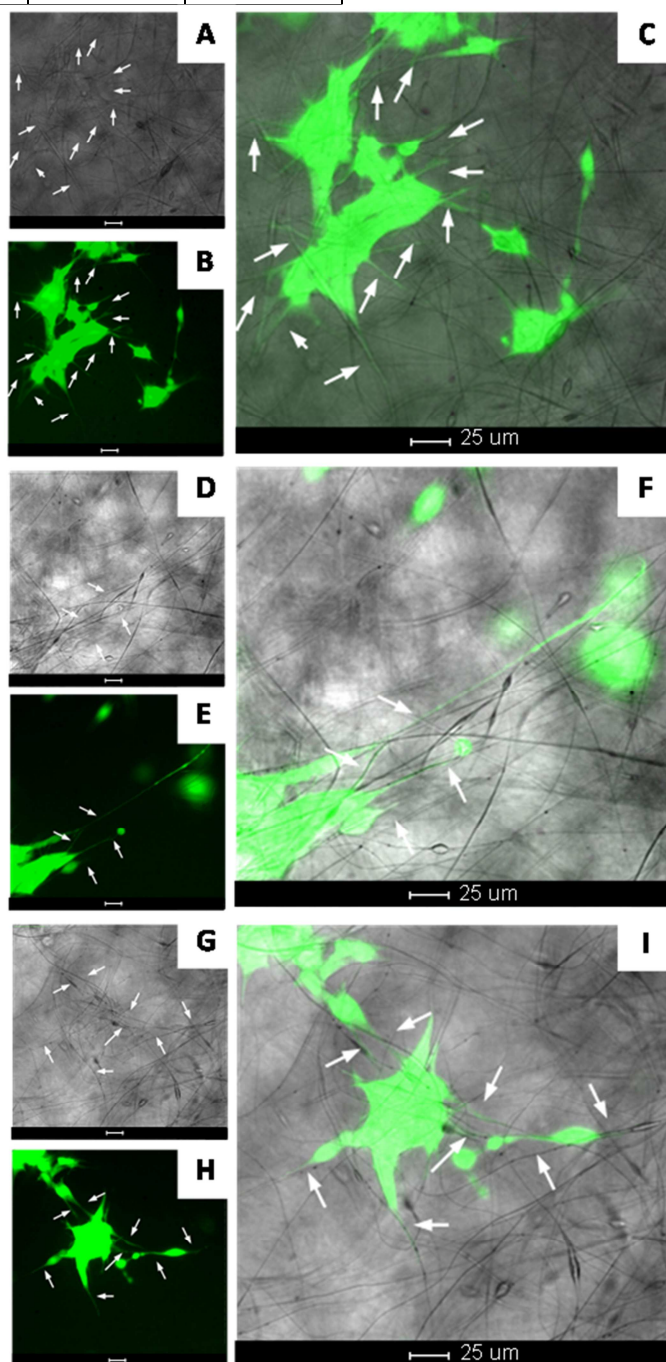| % of cell death | DAY0 | DAY2 | DAY2 RA |
|---|---|---|---|
| CNT-PLLA | 18.06% | 4.52% | 4.06% |
| eCNT-PLLA | 23.45% | 7.48% | 7.44% |
| ePLLA | 22.01% | 7.97% | 7.59% |
| CTRL | 19.59% | 3.86% | 3.34% |



**Fig. 5 - SH-SY5Y cells extend neurites following the scaffold fiber orientation. (A), (D), (G), bright field images of the eCNT-PLLA scaffold; (B), (E), (H), fluorescent images of RA treated SH-SY5Y cells stained with Calcein-**

**AM; (C), (F), (I), superimposition of the fluorescent and corresponding bright field images. White arrows indicate neurites following the scaffold fibers orientation. Image magnification is 32X.**

results. Such a remarkable effect on a PNC material with only 0.25% w/w nanofiller content is a sign of the high quality of the nanodispersion achieved, mainly thanks to the MWCNT chemical functionalization with 4-methoxyphenyl substituent. In fact, for similar PNCs, in which oxidized MWCNTs were dispersed in a PLLA matrix, a similar temperature difference was found, but the nanofiller percentage was one order of magnitude higher (2%) [26]. In both samples it is evident an endothermic peak around 60 °C due to relaxation of the strain within polymer chains, which is more pronounced in the fibrous material possibly due to a certain anisotropy of the sample [28].

We compared eCNT-PLLA with ePLLA and CNT-PLLA for both biocompatibility and neuritogenic properties. No difference in cell proliferation and viability was found when growing cells onto the three different scaffolds or onto the poly-L-lysine coated control wells (Fig. 4a and Table 2). However, cells better adhere onto eCNT-PLLA (~66%) than onto ePLLA (~53%) (Fig. 4B). Furthermore, the total neurite length is significantly increased in samples seeded onto eCNT-PLLA, either in presence or in absence of RA stimulation (Fig. 4C). These results highlight an improved adhesion and differentiation of cells growing onto eCNT-PLLA, possibly due to the combination of

two factors. First, the fibrous morphology of the scaffold, with fibers diameters partially overlapping the diameter range of both axons (80 nm to 20 µm) [29] and collagen fibrils (260-410 nm) [30]. Second, the presence of CNTs that (i) lower scaffold resistance in the bulk (Tab S1) and, most important, can induce beneficial effects at the nanoscale based on their electronic properties [20,31,32] and (ii) can provide sites for cellular anchorage and guidance of cytoskeletal extensions thanks to their nanotopography [33-35].

Indeed, the superimposition (Figure 5 C, F, I) of the fluorescent images of the cells (Figure 6 B, E, H) stained with a cytoplasmatic dye and the bright field images of the corresponding portion of the scaffold (Figure 5 A, D, G) shows that the newly formed neurites elongate following the direction of fiber orientation. This is a strong indication that the scaffold topography guides cells outgrowth and opens up the bright perspective of obtaining a polarized neurites outgrowth and elongation upon previous fibers alignment.

## 4. Conclusions

In conclusion, we have reported on the use of MWCNT-PhOMe as nanofiller into a PLLA matrix for the preparation of a PNC fibrous

scaffold boosting neurite outgrowth and neuronal cell differentiation. The functionalization of pristine CNSs allowed us to achieve a good dispersion of the nanofiller within the polymer solution used to obtain nanofibers through an electrospinning process. We have determined the best conditions to afford in high efficiency a fiber network with a homogeneous morphology. Furthermore, regions of well- dispersed CNTs aligned along fibers axes are evident by TEM analysis. A relevant thermal feature emerged for the material, namely a significant effect on crystallization temperature, which, to the best of our knowledge, is so far unreported at such a low weight percentage of nanofillers content.

We have tested the biological properties of the resulting functional scaffold in terms of biocompatibility and neuritogenesis. A synergy between the fibrous morphology and the presence of well-dispersed CNTs within the polymer matrix has emerged, which paves the way to further develop CNT fibrous scaffolds for neural engineering applications and discloses the possibility of inducing stem cells differentiation toward the neuronal lineage. Furthermore, the here demonstrated activity of the scaffold for neuronal differentiation, even at very low content of CNTs, largely mitigates concerns associated to carbon nanomaterials cytotoxicity.

**Acknowledgements**

**Appendix A. Supplementary data**

This document file contains supplementary information (S. I.).

REFERENCES

[1]     Chen G-Q, Patel MK. Plastics Derived from Biological Sources: Present and Future: A Technical and Environmental Review. Chem Rev 2012;112(4):2082-99.
[2]     Tsuji H. Poly(lactide) Stereocomplexes: Formation, Structure, Properties, Degradation, and Applications. Macromol Biosci 2005;5(7):569-97.
[3]     Hu Y, Shenderova OA, Hu Z, Padgett CW, Brenner DW. Carbon nanostructures for advanced composites. Rep Prog Phys 2006;69(6):1847.
[4]     Grady BP. Carbon Nanotube-Polymer Composites: Manufacture, Properties, and Applications: Wiley 2011.
[5]     Jun Han Z, Rider AE, Ishaq M, Kumar S, Kondyurin A, Bilek MMM, et al. Carbon nanostructures for hard tissue engineering. RSC Adv 2013;3(28):11058-72.
[6]     Saito N, Haniu H, Usui Y, Aoki K, Hara K, Takanashi S, et al. Safe Clinical Use of Carbon Nanotubes as Innovative Biomaterials. Chem Rev 2014;114(11):6040-79.
[7]     Scapin G, Salice P, Tescari S, Menna E, De Filippis V, Filippini F. Enhanced neuronal cell differentiation combining biomimetic peptides and a carbon nanotube-polymer scaffold. Nanomed-Nanotechnol Biol Med 2015;11(3):621-32.
[8]     Cellot G, Cilia E, Cipollone S, Rancic V, Sucapane A, Giordani S, et al. Carbon nanotubes

might improve neuronal performance by favouring electrical shortcuts. Nat Nano 2009;4(2):126-33.

[9] Mattson M, Haddon R, Rao A. Molecular functionalization of carbon nanotubes and use as substrates for neuronal growth. J Mol Neurosci 2000;14(3):175-82.

[10] Bianco A. Graphene: Safe or Toxic? The Two Faces of the Medal. Angew Chem-Int Edit 2013;52(19):4986-97.

[11] Smart SK, Cassady AI, Lu GQ, Martin DJ. The biocompatibility of carbon nanotubes. Carbon 2006;44(6):1034-47.

[12] Salice P, Fabris E, Sartorio C, Fenaroli D, Figà V, Casaletto MP, et al. An insight into the functionalisation of carbon nanotubes by diazonium chemistry: Towards a controlled decoration. Carbon 2014;74(0):73-82.

[13] Bianco A, Kostarelos K, Prato M. Making carbon nanotubes biocompatible and biodegradable. Chem Commun 2011;47(37):10182-8.

[14] Salice P, Fenaroli D, De Filippo CC, Menna E, Gasparini G, Maggini M. Efficient functionalization of carbon nanotubes: an opportunity enabled by flow chemistry. Chim Oggi-Chem Today 2012;30(6):37-9.

[15] Sen R, Zhao B, Perea D, Itkis ME, Hu H, Love J, et al. Preparation of Single-Walled Carbon Nanotube Reinforced Polystyrene and Polyurethane Nanofibers and Membranes by Electrospinning. Nano Lett 2004;4(3):459-64.

[16] Holmes B, Fang X, Zarate A, Keidar M, Zhang LG. Enhanced human bone marrow mesenchymal stem cell chondrogenic differentiation in electrospun constructs with carbon nanomaterials. Carbon 2016;97(0):1-13.

[17] Gnavi S, Fornasari BE, Tonda-Turo C, Ciardelli G, Zanetti M, Geuna S, et al. The influence of electrospun fibre size on Schwann cell behaviour and axonal outgrowth. Materials Science and Engineering: C 2015;48(0):620-31.

[18] Landers J, Turner JT, Heden G, Carlson AL, Bennett NK, Moghe PV, et al. Carbon Nanotube Composites as Multifunctional Substrates for In Situ Actuation of Differentiation of Human Neural Stem Cells. Adv Healthc Mater 2014;3(11):1745-52.

[19] Lizundia E, Sarasua JR, D'Angelo F, Orlacchio A, Martino S, Kenny JM, et al. Biocompatible Poly(L-lactide)/MWCNT Nanocomposites: Morphological Characterization, Electrical Properties, and Stem

Cell Interaction. Macromol Biosci 2012;12(7):870-81.

[20] Lovat V, Pantarotto D, Lagostena L, Cacciari B, Grandolfo M, Righi M, et al. Carbon Nanotube Substrates Boost Neuronal Electrical Signaling. Nano Lett 2005;5(6):1107-10.

[21] Bareket-Keren L, Hanein Y. Carbon nanotube-based multi electrode arrays for neuronal interfacing: progress and prospects. Front Neural Circuits 2013;6:122.

[22] Chen Y-S, Hsiue G-H. Directing neural differentiation of mesenchymal stem cells by carboxylated multiwalled carbon nanotubes. Biomaterials 2013;34(21):4936-44.

[23] Lopes FM, Schröder R, Júnior MLCdF, Zanotto-Filho A, Müller CB, Pires AS, et al. Comparison between proliferative and neuron-like SH-SY5Y cells as an in vitro model for Parkinson disease studies. Brain Res 2010;1337(0):85-94.

[24] D'Este M, De Nardi M, Menna E. A co-functionalization approach to soluble and functional Single-Walled Carbon Nanotubes. Eur J Org Chem 2006(11):2517-22.

[25] Silverajah VSG, Ibrahim NA, Yunus WMZW, Hassan HA, Woei CB. A Comparative Study on the Mechanical, Thermal and Morphological Characterization of Poly(lactic acid)/Epoxidized Palm Oil Blend. Int J Mol Sci 2012;13(5):5878-98.

[26] Papageorgiou GZ, Achilias DS, Nanaki S, Beslikas T, Bikiaris D. PLA nanocomposites: Effect of filler type on non-isothermal crystallization. Thermochim Acta 2010;511(1–2):129-39.

[27] Zhai W, Ko Y, Zhu W, Wong A, Park C. A Study of the Crystallization, Melting, and Foaming Behaviors of Polylactic Acid in Compressed $CO_2$. Int J Mol Sci 2009;10(12):5381-97.

[28] Hatakeyama T, Quinn FX. Thermal Analysis: Fundamentals and Applications to Polymer Science: Wiley 1999.

[29] Debanne D, Campanac E, Bialowas A, Carlier E, Alcaraz G. Axon Physiology. Physiol Rev 2011;91(2):555-602.

[30] Dvir T, Timko BP, Kohane DS, Langer R. Nanotechnological strategies for engineering complex tissues. Nat Nano 2011;6(1):13-22.

[31] Gabay T, Ben-David M, Kalifa I, Sorkin R, Abrams ZR, Ben-Jacob E, et al. Electro-chemical and biological properties of carbon nanotube based multi-electrode arrays. Nanotechnology 2007;18(3).

[32]    Keefer EW, Botterman BR, Romero MI, Rossi AF, Gross GW. Carbon nanotube coating improves neuronal recordings. Nat Nanotechnol 2008;3(7):434-9.

[33]    Lee JH, Lee J-Y, Yang SH, Lee E-J, Kim H-W. Carbon nanotube–collagen three-dimensional culture of mesenchymal stem cells promotes expression of neural phenotypes and secretion of neurotrophic factors. Acta Biomater 2014;10(10):4425-36.

[34]    Hu H, Ni YC, Montana V, Haddon RC, Parpura V. Chemically functionalized carbon nanotubes as substrates for neuronal growth. Nano Lett 2004;4(3):507-11.

[35]    Gabay T, Jakobs E, Ben-Jacob E, Hanein Y. Engineered self-organization of neural networks using carbon nanotube clusters. Physica a-Statistical Mechanics and Its Applications 2005;350(2-4):611-21.

**Supplementary Data**

# Covalent functionalization enables good dispersion and anisotropic orientation of multi-walled carbon nanotubes in a poly(L-lactic acid) electrospun nanofibrous matrix boosting neuronal differentiation

Nicola Vicentini,[a] Teresa Gatti,[a] Patrizio Salice,[a] Giorgia Scapin,[b] Carla Marega,[a] Francesco Filippini,[b] Enzo Menna[a,*]

[a] Dipartimento di Scienze Chimiche, Università di Padova, via F. Marzolo 1, 35131, Padova, Italy

[b] Dipartimento di Biologia, Università di Padova, via U. Bassi 58/B, 35131, Padova, Italy
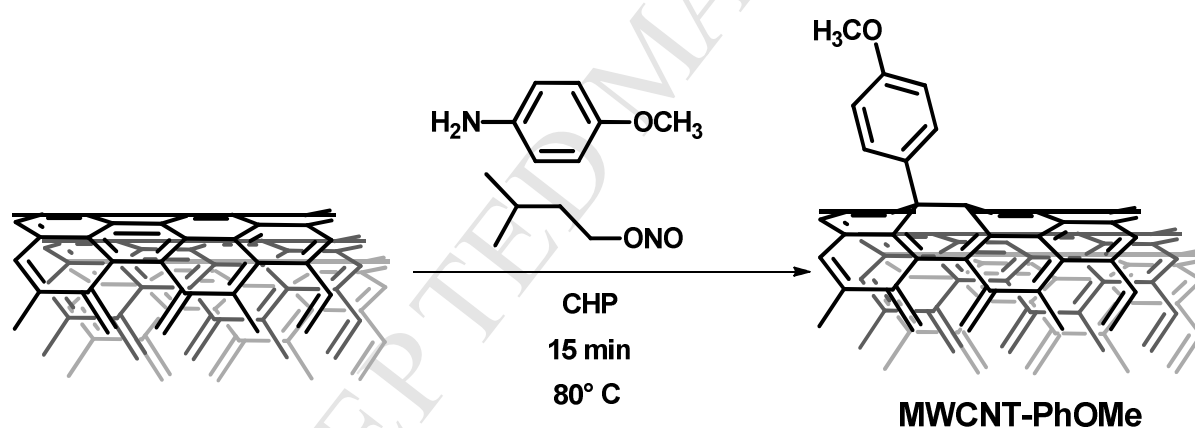
**Fig. S1** – Synthetic route towards MWCNT-PhOMe

**PLLA**

**CHCl₃**

**Stirring**

**MWCNT-PhOMe**

**DMF**

**Sonication**

**Stirring**

**Centrifugation**

**MWCNT-PhOMe@PLLA**

**CHCl₃:DMF 9:1**
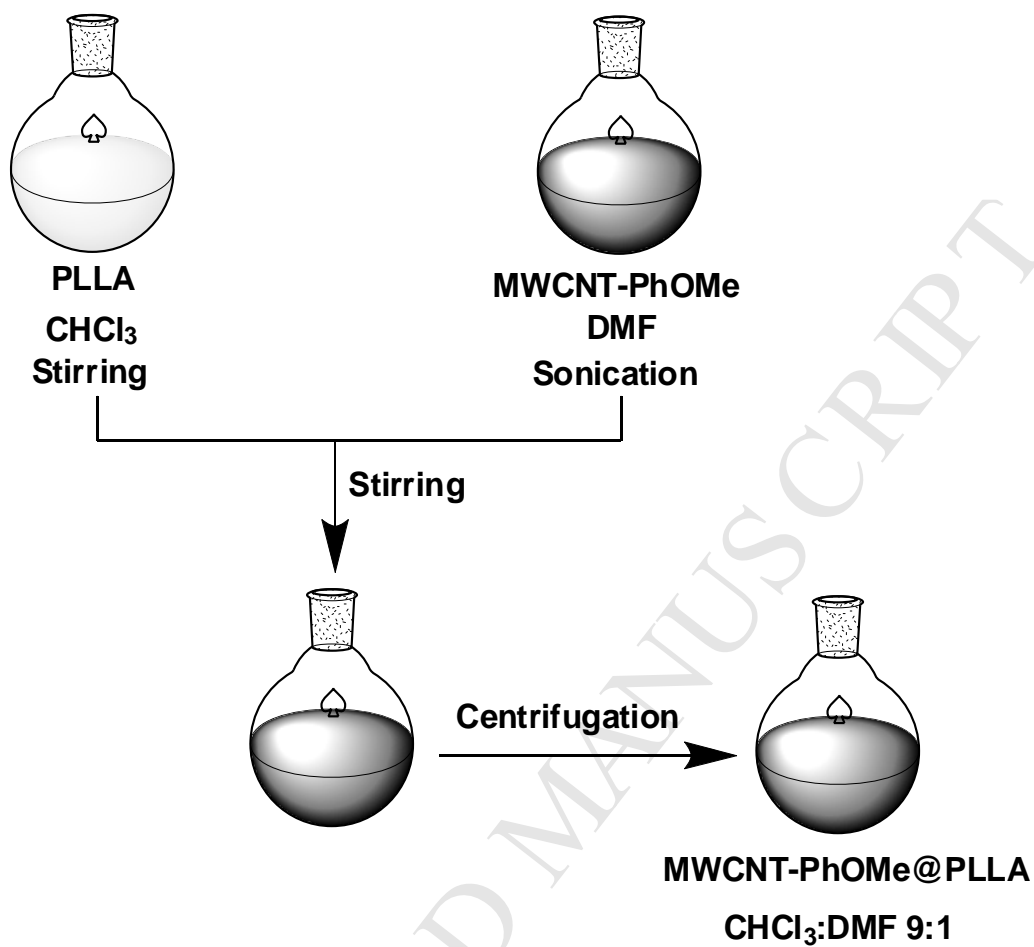
**Fig. S2 –** Schematic representation of the preparation of MWCNT-PhOMe@PLLA PNC solutions used for electrospinning.
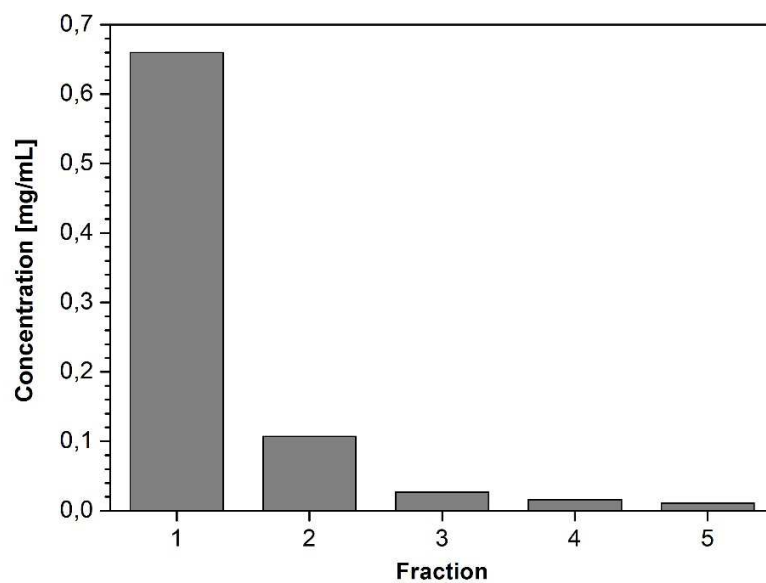
**Fig. S3 –** Concentration of MWCNT-PhOMe subsequently extracted fractions in CHCl$_3$.
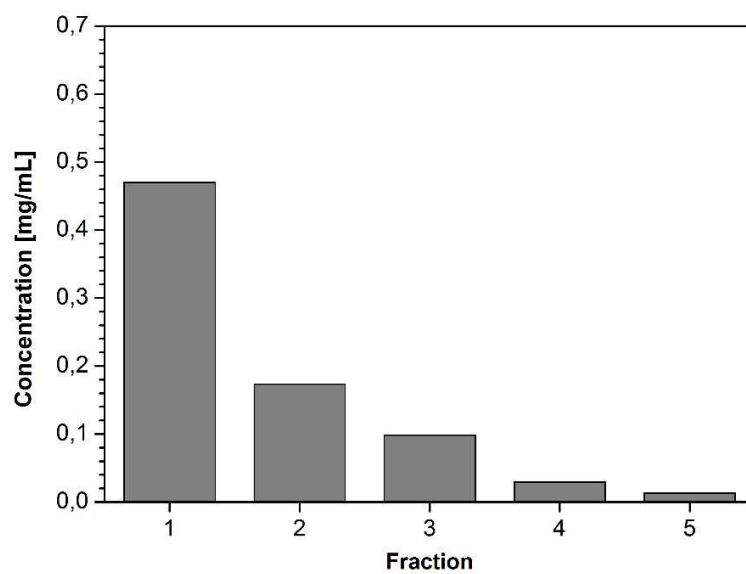


**Fig. S4 –** Concentration of MWCNT-PhOMe subsequently extracted fractions in DMF.

Thermogravimetric analysis (TGA) was performed on a Q5000IR TGA (TA instruments) under air and under a nitrogen flow by previously performing an isotherm at 100 °C for 10 min followed by heating at 10 °C min$^{-1}$ until 1000 °C.
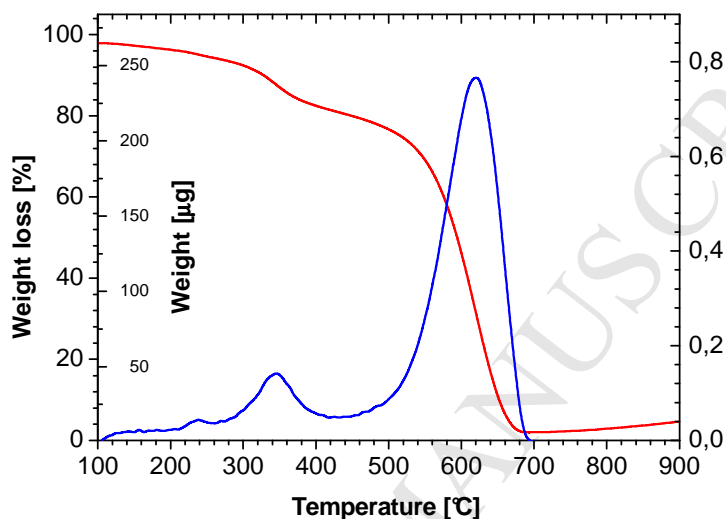


**Fig. S5 –** Thermograms of MWCNT-PhOMe first fraction extracted in CHCl$_3$ under air. Red line represents weight percentage loss (left axis) and blue line the corresponding derivative (right axis).
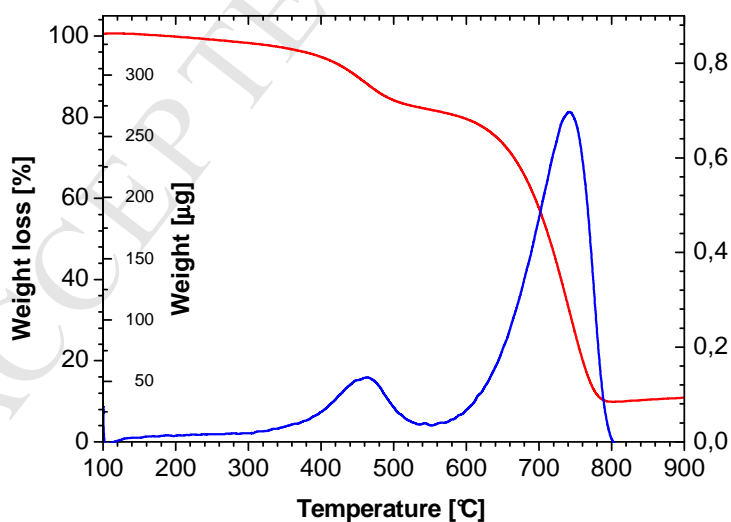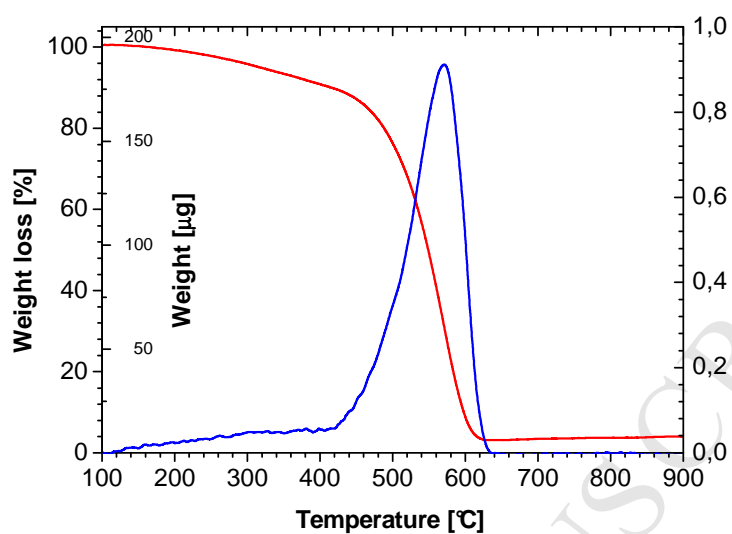


**Fig. S6 –** Thermograms of MWCNT-PhOMe first fraction extracted in CHCl$_3$ under nitrogen. Red line represents weight percentage loss (left axis) and blue line the corresponding derivative (right axis).

S4

**Fig. S7 –** Thermograms of MWCNT-PhOMe first fraction extracted in DMF under air. Red line represents weight percentage loss (left axis) and blue line the corresponding derivative (right axis).
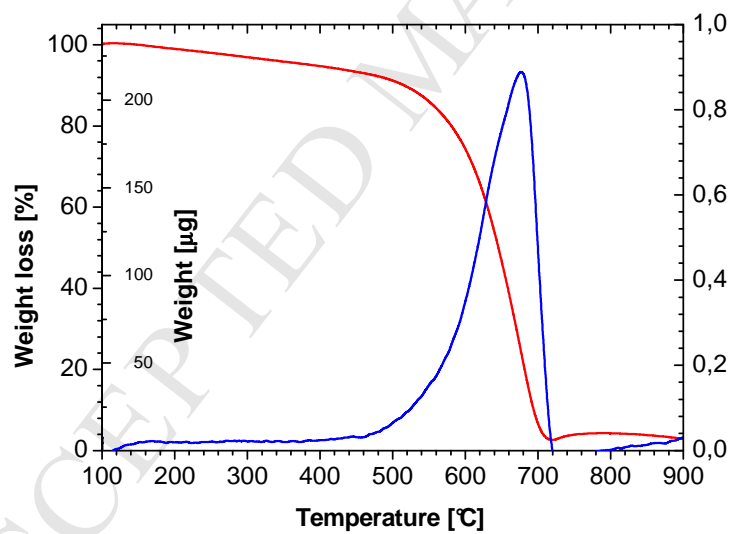


**Fig. S8 –** Thermograms of MWCNT-PhOMe first fraction extracted in DMF under nitrogen. Red line represents weight percentage loss (left axis) and blue line the corresponding derivative (right axis).

S5

Raman spectra of MWCNT-PhOMe samples drop-casted on glass micro slides and heated up to remove the solvent were obtained with an Invia Renishaw Raman microspectrometer (50 × objective) using the 633 nm line of a He-Ne laser.
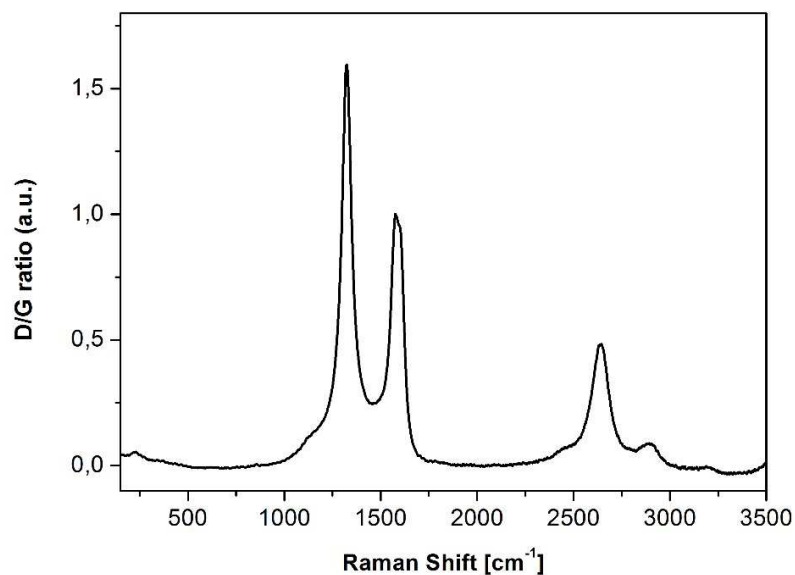


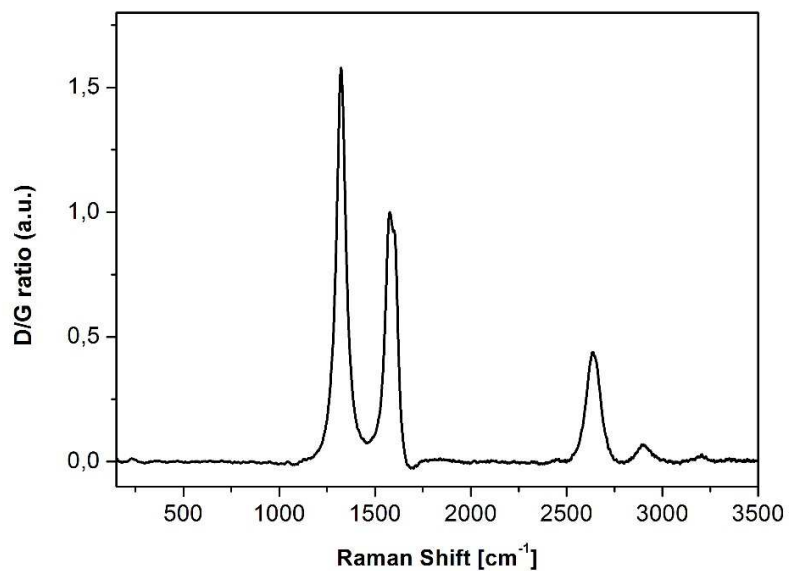**Fig. S9 –** Raman spectrum of MWCNT-PhOMe first fraction extracted in CHCl₃.



**Fig. S10 –** Raman spectrum of MWCNT-PhOMe first fraction extracted in DMF.
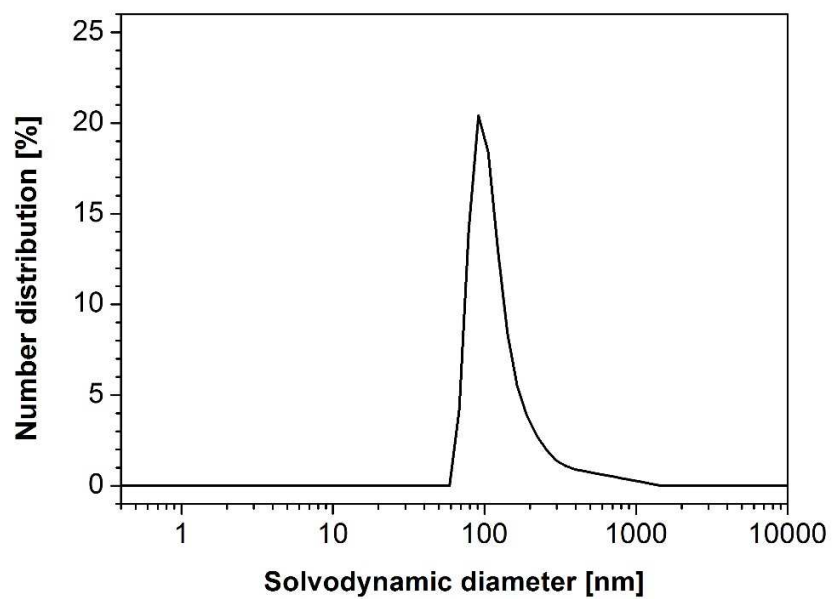
**Fig. S11** – DLS analysis of MWCNT-PhOMe first fraction extracted in CHCl$_3$.
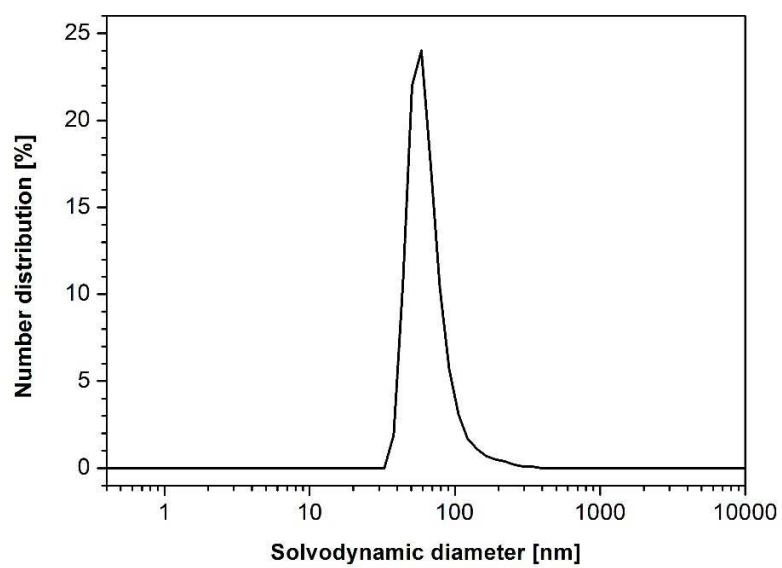


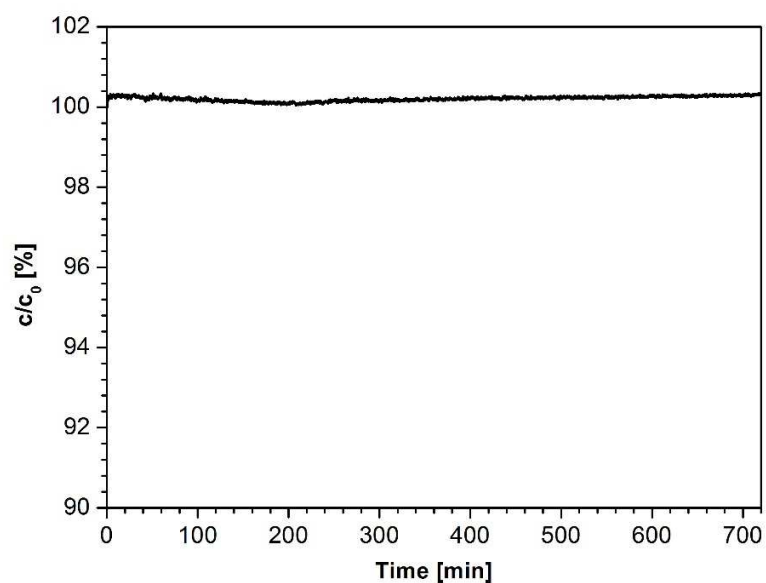**Fig. S12** – DLS analysis of MWCNT-PhOMe first fraction extracted in DMF.

**Fig. S13 –** In time evolution of concentration percentage for MWCNT-PhOMe first fraction extracted in CHCl$_3$.
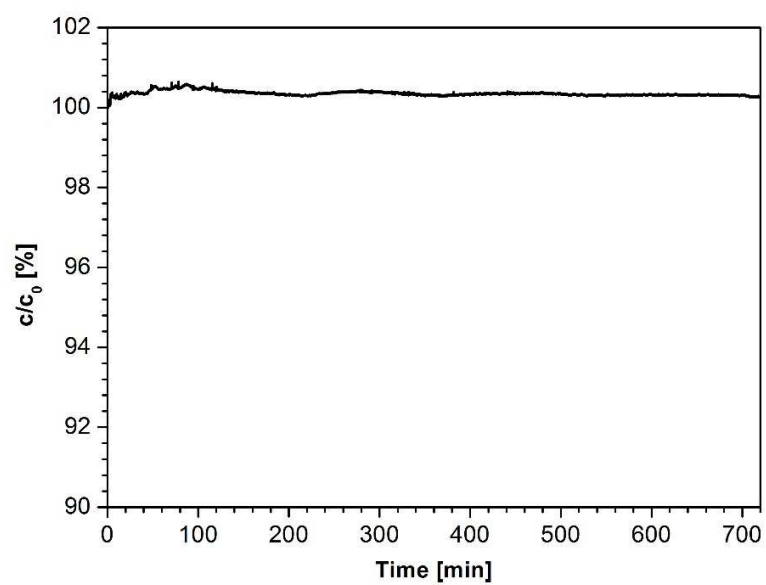


**Fig. S14 –** In time evolution of concentration percentage for MWCNT-PhOMe first fraction extracted in DMF.
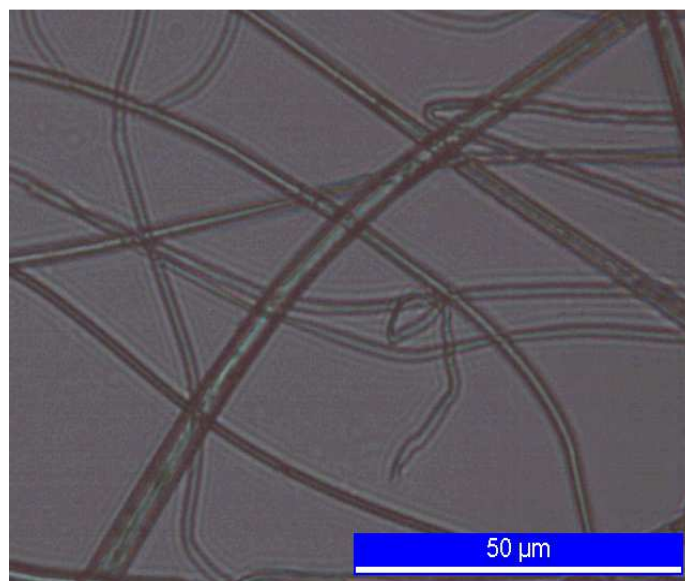
**Fig. S15 –** Optical microscopy image of electrospun nanofibers obtained from 12% MWCNT-PhOMe@PLLA solution.
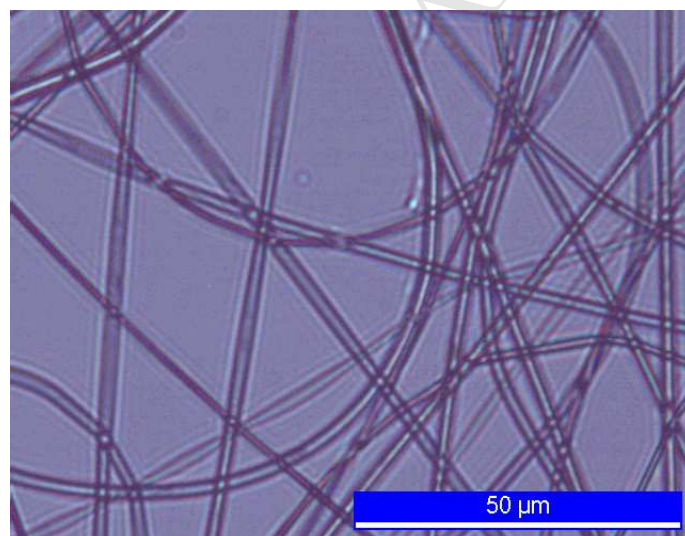


**Fig. S16 –** Optical microscopy image of electrospun nanofibers obtained from 10% MWCNT-PhOMe@PLLA solution.

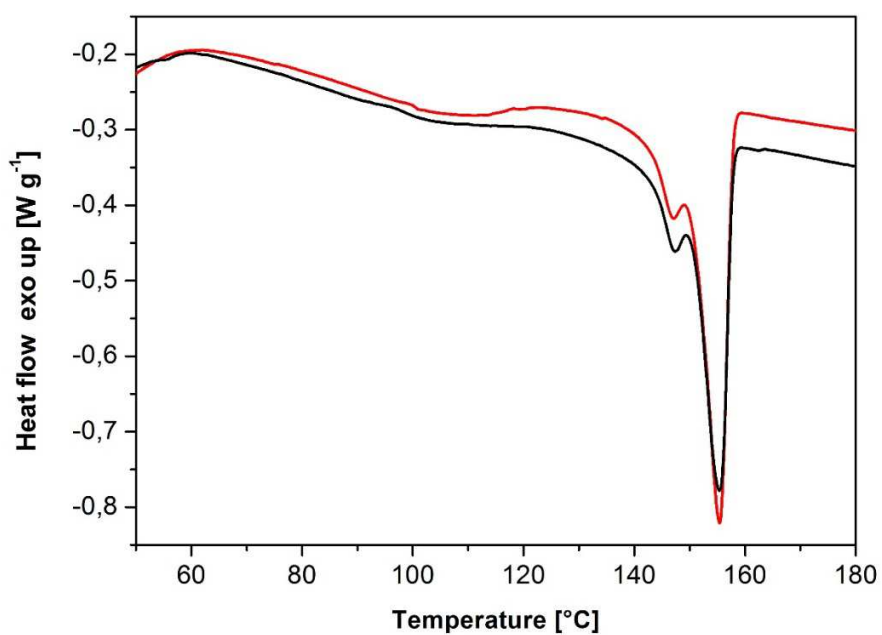**Fig. S17 –** DSC heating traces of PLLA (black line) and CNT-PLLA (red line) obtained at 1°C min$^{-1}$ rate.

**Tab. S1 –** Resistance data of ePLLA and eCNT-PLLA fibers. Data obtained with Keithley's Electrometer High Resistance Meter (model 6517B) and the Keithley's Resistivity Test Chamber (model 8009).

| | ePLLA | eCNT-PLLA |
|---|---|---|
| Resistance [Ω] | 3.11 X 10$^{15}$ | 5.08 X 10$^{14}$ |

**Biological tests: experimental details**

SH-SY5Y cells were cultured with Dulbecco's Modified Eagle Medium/Nutrient Mixture F-12 (DMEM/F-12) + GlutaMAX™ (Invitrogen Life Technologies) supplemented with 10% heat-inactivated foetal bovine serum (FBS, Euroclone) and 25μg/ml gentamicin (Sigma-Aldrich) (growth medium), in a humidified atmosphere of 5% of $CO_2$ in air at 37 °C. Cells were maintained by subculturing 900000 cells per 25 cm² flask (Sarstedt) every 2 days (once they reached 90% confluence). Round slices (13 mm diameter) of CNT-PLLA sheets and eCNT-PLLA/ePLLA fibre-covered coverslips were sterilized by UV irradiation and positioned into 24-well plates. Scaffolds were pre-incubated for 24 hours in the growth medium prior to seeding cells (at 15000/well density) in the growth medium onto either the scaffolds or the well bottoms coated with a gelatine (Sigma-Aldrich, porcine skin 0.005% in milliQ water)/poly-L-lysine (Invitrogen Life Technologies, 1μg/ml) solution (control). Twenty-four hours after cell seeding (day 0), the culture medium was replaced by the differentiation medium (DMEM/F-12 medium supplemented with 2% heat-inactivated FBS, 25μg/ml gentamicin and 10 μM all-*trans*-retinoic acid (RA) (Sigma-Aldrich). In undifferentiated control samples, Dimethyl sulfoxide (DMSO; Sigma) was added as equivalent amount (in which RA is dissolved).

Analysis of cell viability/proliferation and neuronal differentiation were performed as previously reported [Scapin G et al. Nanomed-Nanotechnol Biol Med 2015;11(3):621-32.]. Briefly, Resazurin reduction assay was used to quantify metabolically active living cells and thus to monitor the effects of scaffolds on cell proliferation. The assay is based on the reduction of the indicator dye, resazurin (not fluorescent) to the highly fluorescent resorufin (Ex. 569 nm, Em. 590 nm) by viable cells. Non-viable cells rapidly lose their capacity to reduce resazurin and, thus, to emit fluorescent signals anymore. The culture medium was replaced by 500 µL of resazurin solution (Resazurin Sigma 15 μg/mL in growth medium without phenol red) and cells were incubated for 4 h in the dark at 37°C, 5% $CO_2$. Then, 200 μL of resazurin solution were removed twice from each well and transfer to a 96 well plate (technical duplicates). Fluorescence, directly correlated with cell quantity, was detected using a plate reader (Ascent Fluoroscan, excitation 540 nm, emission 590 nm). Background values from blank samples were subtracted and average values for the duplicates calculated. Cell proliferation was calculated from a calibration curve by linear regression using Microsoft Excel. Resazurin assay was also

used for testing cell ability to adhere to the scaffolds. 24 h after cell seeding, scaffolds were removed from the original wells and positioned into clean ones. Both wells were incubated with resazurin solution to quantify the number of cells adherent to scaffold or to well bottom. The CytoTox-ONE™ Homogeneous Membrane Integrity Assay (Promega) was used to quantify the lactate dehydrogenase (LDH) release by cells that lose membrane integrity. Briefly, 100 μL of culture medium were transferred to a new 96 well plate. 50 μL of the reaction solution from the kit, containing the detection dye and the catalyst were then added to culture supernatants and fluorescence was measured after 10 minutes in a plate reader (Ascent Fluoroscan, excitation 540 nm, emission 590 nm). Background values from wells without cells were subtracted and average values for the duplicates calculated. Cell death was calculated from a calibration curve by linear regression after 100% cell lysis of known cell quantities. Cytotoxicity was then calculated according to the following equation: Cytotoxicity (%) = (number of dead cells)/(n of dead cells + number of living cells) x100. Neurite outgrowth was measured after staining the cells with calcein acetoxymethyl ester (Calcein-AM, Biotium), a non-fluorescent cell permeable compound that when hydrolyzed by intracellular esterases in live cells converts to the strongly green fluorescent calcein (Ex. 490 nm, Em. 539 nm). Briefly, cells were incubated with calcein-AM (2 μM in HBSS, Hank's Balanced Salt Solution, Invitrogen) for 30 minutes in dark at 37°C and 5% $CO_2$ and visualized under a fluorescent microscope (Leica DM4000b) using GFP filter. Each experiment was performed in duplicate (two wells per conditions). Five images/well were recorded (ten images for each condition), taken with a 20X objective. The first field was selected in the centre of the well. The next fields were selected in the four directions (N, S, W, E) from the first field. Neurite length was measured using LAS AF lite software (Leica) by tracing the trajectory of the neurite from the tip to the junction between the neurite and cell body. If a neurite exhibited branching, the measurement from the end of the longest branch to the soma was recorded, then each branch was measured from the tip of the neurite to the neurite branch point. The neuritogenic properties were analyzed in terms of total neurite length/no. of cells (adding the lengths of all the processes of each cell divided by cell number). Only neurites longer than 50 μm were considered. Statistical analysis was performed using paired Student's t test, and results were considered significant when p< 0.05. Values are expressed as mean ± standard error of the mean (M ± SEM).